EM Implosion Memos

Memo 42

May, 2010

The truncated four feed-arm configuration with switch cones (T4FASC) and a spherical pressure vessel

Prashanth Kumar, Serhat Altunc, Carl E. Baum, Christos G. Christodoulou and Edl Schamiloglu
University of New Mexico
Department of Electrical and Computer Engineering
Albuquerque, NM 87131

Abstract

In this paper, numerical simulations are used to investigate the truncated four feed-arm configuration with the switch cones (T4FASC) and a spherical pressure vessel. The near-field electric field responses and the focal impulse waveforms are compared for cylindrical and spherical hydrogen chamber geometries.

1 Introduction

Of the various switch configurations investigated in [1], the T4FASC and 150 Ω VBCS designs were considered the most promising. The next stage in the design of the switch system is to include the gas chamber, pressure vessel, and launching lens. These components are necessary as 100 kV or more will be applied across the switch gap. The gas chamber typically contains hydrogen or SF_6 under high pressure. In this paper, hydrogen is used as an example.

The launching lens is required to ensure that spherical TEM waves originate from the source. Previous attempts focused on designing such a lens when the source and focal points were spatially isolated [2–5]. The location of the geometric center of the switch cones at the first focal point greatly simplifies the design. The design is further simplified if one considers a *spherical* pressure vessel which also serves to function as the launching lens. Then the switch system consists of only three components: 1) switch cones and guiding structures 2) hydrogen chamber (HC) and 3) spherical pressure vessel (SPV).

The maximum dimension of the HC is typically $\ll ct_\delta$. The HC can be cylindrical or spherical, but the choice of geometry is not obvious. From an electromagnetic perspective, a spherical chamber is preferred as it better conserves the sphericity of the waves, at least in the (early) times of interest. However, one might argue that the size of the HC is too small to signficantly distort the spherical wavefront originating from the source. This paper compares cylindrical and spherical hydrogen chambers with a spherical pressure vessel for the T4FASC configuration. A similar comparison is made for the 150 Ω VBCS design in the next memo.

2 Setup

A feed arm length of $l_{\text{FA}} \approx 18.0$ cm with a loft of length $y \approx 8.0$ cm is used. These lengths correspond to the maximum peak focal impulse amplitudes in [6].

The switch cones are enclosed in the HC, $\epsilon_{r_{\text{hc}}} = 1.0$, which is surrounded by a SPV, $\epsilon_{r_{\text{pv}}} = 3.7$. A spherical oil container, $\epsilon_{r_{\text{oil}}} = 2.25$ (transformer oil), surrounds the PV and is used to denote the oil "bath" that will surround the switch and feed-arms in the final, experimental realization of the design.

To provide structural support to the PV a cylindrical section must be added to the base of the switch cones. The addition of this cylindrical support section (CSS) to the T4FASC design is investigated first. The SPV and HC are then incoorporated into this design. As a first guess, a height of $H_{\text{css}} = 0.5$ cm is used for the CSS. This height is optimized in a later memo.

2.1 Structure visualization

2.1.1 T4FASC-CSS

Figure 2.1 shows the perspective view of the T4FASC design with the CSS and the reflector. The details of the switch geometry are shown in Fig. 2.2. The geometric center of the switch cones is the first focal point. The impedance of the switch cone is $Z_c = 100$ Ω (bicone impedance $= 2Z_c$), i.e., the half-angle of the cones is, $\theta = 21.37°$.

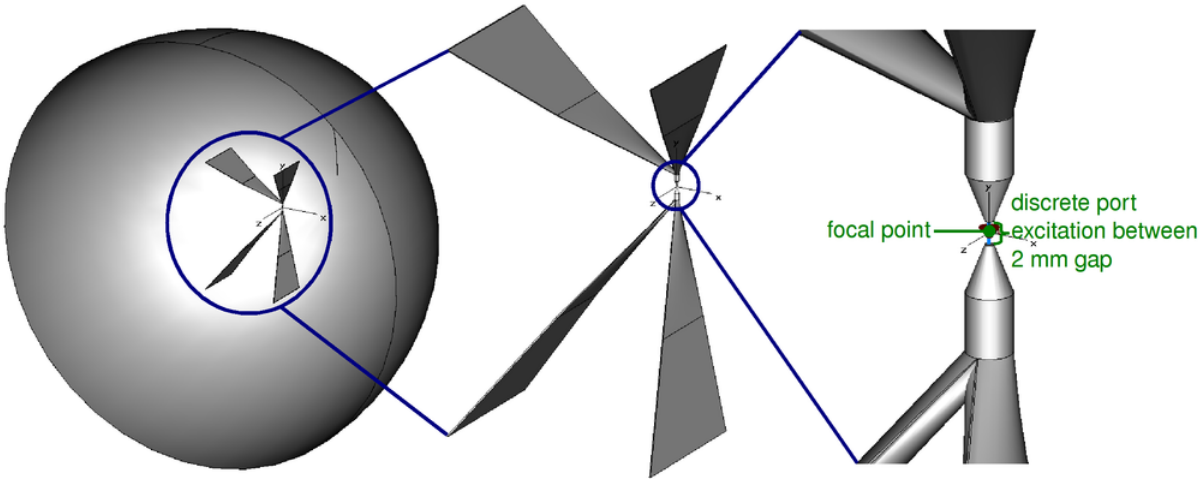

Figure 2.1: Perspective view of T4FASC-CSS configuration with reflector; "Zoomed-in" view showing discrete port excitation.

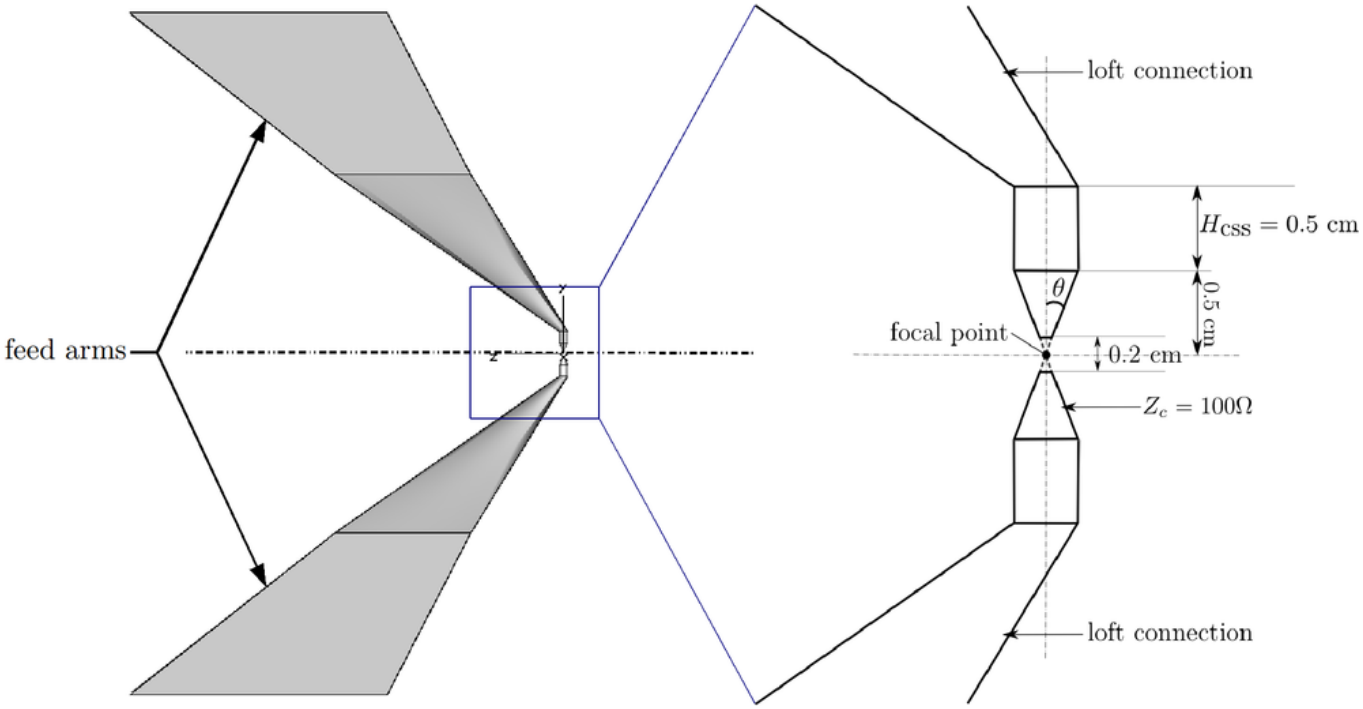

Figure 2.2: Geometrical details and "zoomed-in" side view of switch system for the T4FASC-CSS configuration.

2.1.2 T4FASC-CSS-SPVCHC

Figure 2.3 shows the perspective view of the T4FASC-CSS with the spherical pressure vessel and cylindrical hydrogen chamber (SPVCHC) and the reflector. The details of the switch geometry are shown in Fig. 2.4. All components are centered at the first focal point.

The impedance of the switch cone is $Z_c = 100\ \Omega$ (bicone impedance $= 2Z_c$) *in the pressure*

vessel medium, i.e., the half-angle of the cones is,

$$Z_c^{\text{pv}} = \frac{Z_c^{\text{air}}}{\sqrt{\epsilon_{r_{\text{pv}}}}} = \frac{100\ \Omega}{\sqrt{3.7}} = 51.988\ \Omega \tag{2.1}$$

$$\therefore \theta = 2\ \text{arccot}\left[\exp\left(2\pi Z_c^{\text{pv}}\sqrt{\frac{\epsilon}{\mu}}\right)\right] = 45.583^\circ \tag{2.2}$$

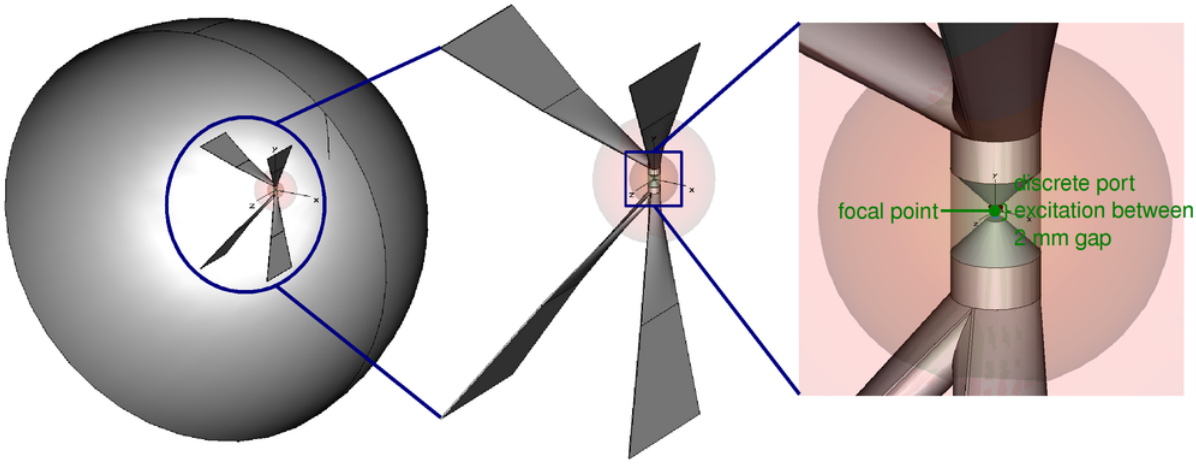

Figure 2.3: Perspective view of T4FASC-CSS-SPVCHC configuration with reflector; "Zoomed-in" view showing discrete port excitation.

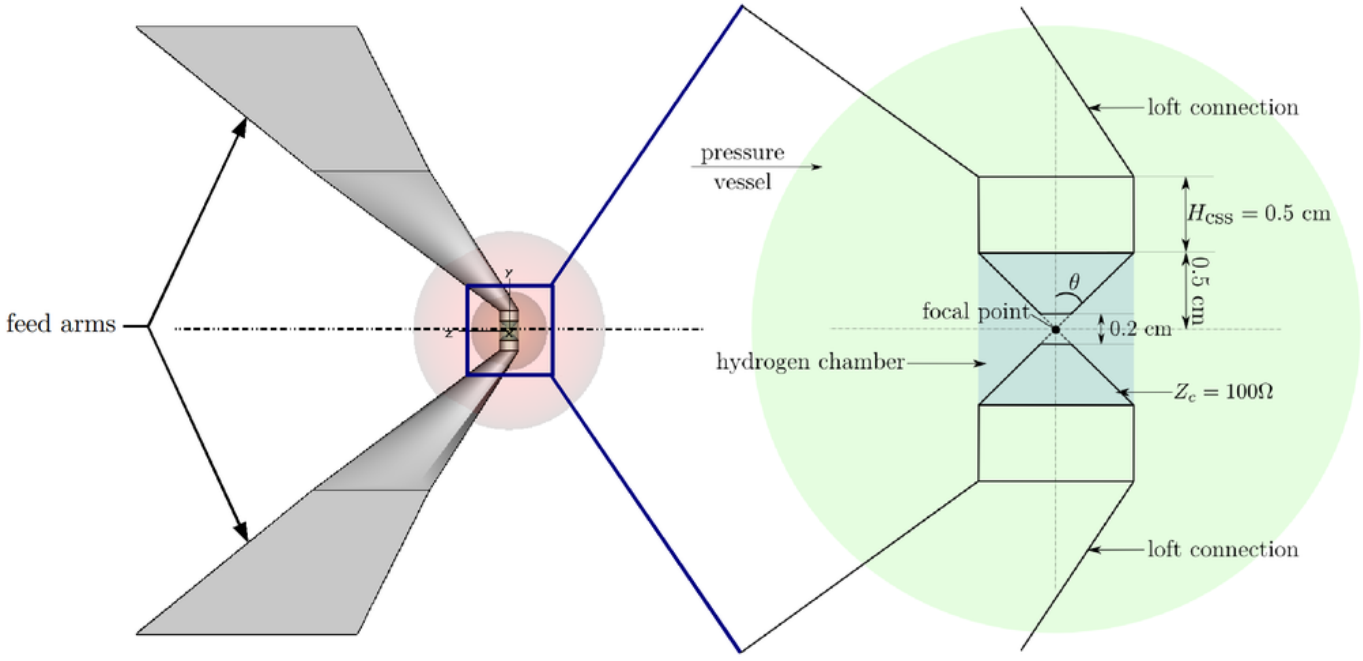

Figure 2.4: Geometrical details and "zoomed-in" side view of switch system for the T4FASC-CSS-SPVCHC configuration.

The physical dimensions of the switch system components are summarized in Table 1.

Table 1: Dimensions of switch system components

Component	Height (cm)	Radius (cm)
switch cone	$h = 0.5$	$r = h \tan\theta$
cylindrical support	$H_{\text{css}} = 0.5$	$r = h \tan\theta$
hydrogen chamber	$h_{\text{hc}} = 1.0$	$r_{\text{hc}} = h \tan\theta$
pressure vessel	–	$r_{\text{pv}} = 2.0$
oil medium	–	$r_{\text{oil}} = 5.0$

2.1.3 T4FASC-CSS-SPVSHC

Figure 2.5 shows the perspective view of the T4FASC-CSS with the spherical pressure vessel and spherical hydrogen chamber (SPVSHC) and the reflector. The details of the switch geometry are shown in Fig. 2.6. The setup is almost identical to the T4FASC-CSS-SPVCHC design.

The dimensions of the switch system components are summarized in Table 2. For the T4FASC-

Table 2: Dimensions of switch system components

Component	Height (cm)	Radius (cm)
switch cone	$h = 0.5$	$r = h \tan\theta$
cylindrical support	$H_{\text{css}} = 0.5$	$r = h \tan\theta$
hydrogen chamber	–	$r_{\text{hc}} = h \sec\theta$
pressure vessel	–	$r_{\text{pv}} = 2.0$
oil medium	–	$r_{\text{oil}} = 5.0$

CSS-SPVCHC and T4FASC-CSS-SPVSHC configurations, note that the electrical height of the CSS is increased, due to the surrounding pressure vessel medium, by a factor of $\sqrt{\epsilon_{r_{\text{pv}}}} = 1.92$ and the electrical length of the loft connections is increased, due to the surrounding oil medium, by a factor of $\sqrt{\epsilon_{r_{\text{oil}}}} = 1.5$.

3 CST parameters

- CST parameters and probe placements are identical to those in [7].
- In all simulations, a discrete port, 1 V, 100 ps, ramp rising step, excitation is applied between a 2 mm gap in the switch cones.

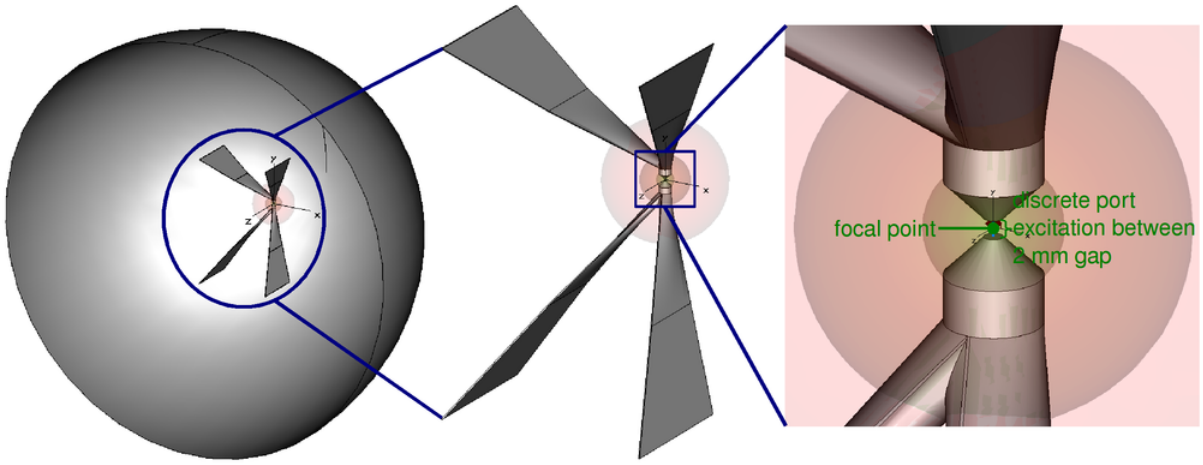

Figure 2.5: Perspective view of T4FASC-CSS-SPVSHC configuration with reflector; "Zoomed-in" view showing discrete port excitation.

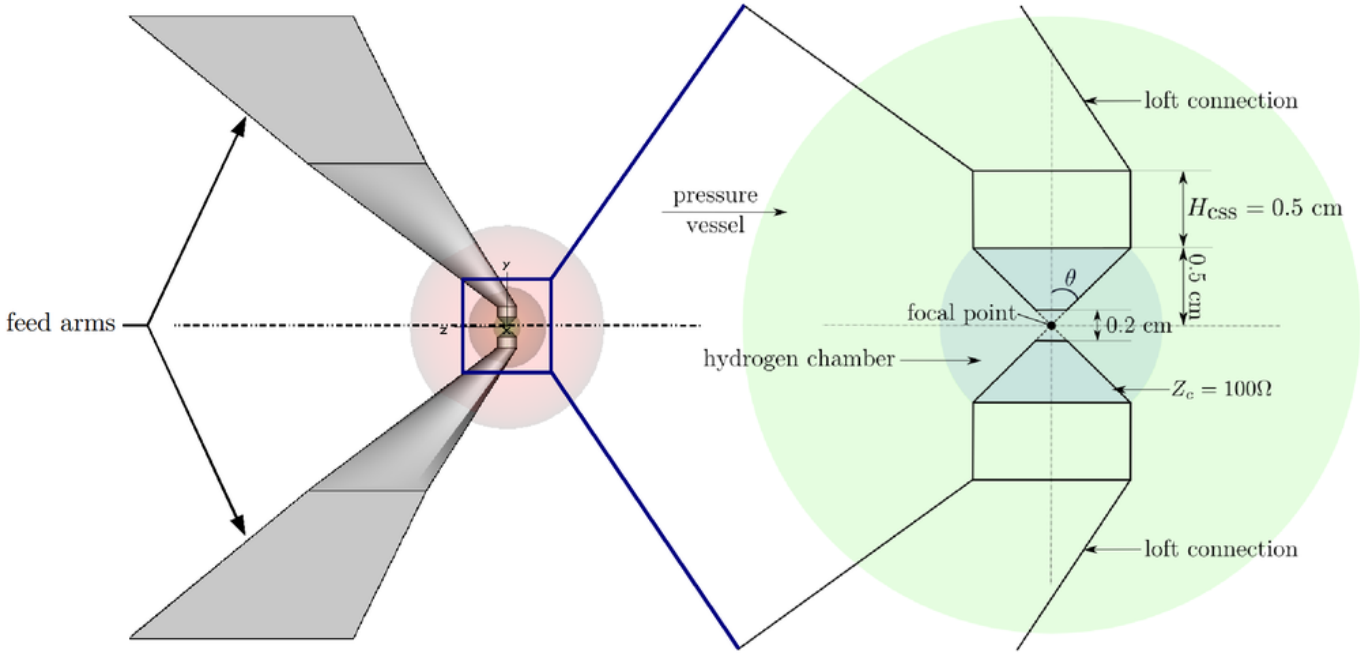

Figure 2.6: Geometrical details and "zoomed-in" side view of switch system for the T4FASC-CSS-SPVSHC configuration.

4 Results

The time spread in the normalized responses, for the T4FASC, T4FASC-CSS-CPVCHC and T4FASC-CSS-CPVCHC configurations, from the near-field electric field probes, are summarized in Table 3 (each response is normalized with respect to its maximum). As expected, the E_ϕ component in the -$yz-$plane and the E_θ component in the $-zx$-plane are zero for all configurations. For the T4FASC-CSS-SPVCHC and T4FASC-CSS-SPVSHC configurations the maximum time spread occurs in the E_θ component in the $-yz$-plane, $\lessapprox 50$ ps. All other components have a time spread

$\lessapprox$ 20 ps. Identical results for the T4FASC-CSS-SPVCHC and T4FASC-CSS-SPVSHC structures leads one to speculate that the geometry of the hydrogen chamber does not significantly affect the electric fields.

Table 3: Summary of the approximate time-spread in the normalized near-field electric field responses for the T4FASC-CSS, T4FASC-CSS-SPVCHC and T4FASC-CSS-SPVSHC configurations.

Component	Time spread (ps)		
	T4FASC-CSS	T4FASC-CSS-SPVCHC	T4FASC-CSS-SPVSHC
E_ϕ: $-yz-$plane	0	0	0
E_θ: $-zx-$plane	0	0	0
E_ϕ: $xy-$plane	≈ 20	$\lessapprox 20$	$\lessapprox 20$
E_θ: $xy-$plane	≈ 20	$\lessapprox 20$	$\lessapprox 20$
E_ϕ: $-zx-$plane	$\lessapprox 30$	$\lessapprox 20$	$\lessapprox 20$
E_θ: $-yz-$plane	$\lessapprox 30$	$\lessapprox 50$	$\lessapprox 50$

The peak focal impulse amplitudes ($E_{\max}$), spot sizes and ΔFWHMs for all configurations are summarized in Table 4. ΔFWHM is the FWHM, of the focal impulse, relative to the 4FASC configuration in [1], i.e., for a configuration, C, $\Delta\text{FWHM}^C = \text{FWHM}^C - \text{FWHM}^{4\text{FASC}}$. ΔFWHM is therefore also indirectly indicative of the time spread. One notes that $E_{\max}$ for the T4FASC-CSS is approximately 0.5 V/m higher than the T4FASC design in [1]. This implies the CSS is beneficial as it enhances $E_{\max}$. For the T4FASC-CSS-SPVCHC and T4FASC-CSS-SPVSHC configurations, $E_{\max}$ is further enhanced due to the surrounding PV and oil chamber. By observing that $E_{\max}$ for the T4FASC-CSS-SPVSHC is approximately 2.13 V/m higher than the T4FASC-CSS-SPVCHC structure one concludes that the HC geometry noticably affects the focal impulse electric field. The spot size is larger with the SPV but this is of less concern than $E_{\max}$. ΔFHWM for the T4FASC-CSS-SPVSHC configuration is less than 15 ps which is within tolerance.

Table 4: Peak focal impulse amplitudes ($E_{\max}$) and spot sizes for the T4FASC-CSS, T4FASC-CSS-SPVCHC and T4FASC-CSS-SPVSHC configurations.

Configuration	$E_{\max}$ (V/m)	ΔFWHM (ps)	Spot diameter (cm)
T4FASC-CSS	7.708	4.271	3.950
T4FASC-CSS-SPVCHC	11.505	21.918	5.093
T4FASC-CSS-SPVSHC	13.762	14.241	4.644

Near-field plots for all configurations are given in Appendix-I. The focal impulse waveforms and the spot sizes are given in Appendix-II.

5 Conclusion

The peak focal impulse amplitude for the T4FASC-CSS-SPVCHC and T4FASC-CSS-SPVSHC is amplified due to the surrounding PV and oil medium. The near-field results for these configurations are similar. However, a higher peak focal impulse amplitude for the T4FASC-CSS-SPVSHC design makes it more attractive for experimental investigation.

References

[1] Prashanth Kumar, Carl E. Baum, Serhat Altunc, Christos G. Christodoulou and Edl Schamiloglu, "Investigation of various switch configurations." EM Implosion Memo 39, Feb. 2010.

[2] Prashanth Kumar, Carl E. Baum, Serhat Altunc, Christos G. Christodoulou and Edl Schamiloglu, "Analytical considerations for curve defining boundary of a non-uniform launching lens." EM Implosion Memo 26, June 2009.

[3] Prashanth Kumar, Carl E. Baum, Serhat Altunc, Christos G. Christodoulou and Edl Schamiloglu, "Simulation results for 3-layer and 6-layer planar non-uniform launching lens." EM Implosion Memo 27, June 2009.

[4] Prashanth Kumar, Carl E. Baum, Serhat Altunc, Christos G. Christodoulou and Edl Schamiloglu, "Derivation of the dielectric constant as a function of angle for designing a conical non-uniform launching lens." EM Implosion Memo 28, June 2009.

[5] Prashanth Kumar, Carl E. Baum, Serhat Altunc, Christos G. Christodoulou and Edl Schamiloglu, "Simulation results for 6-layer and 7-layer conical non-uniform launching lens." EM Implosion Memo 29, June 2009.

[6] Prashanth Kumar, Carl E. Baum, Serhat Altunc, Christos G. Christodoulou and Edl Schamiloglu, "Optimization of the feed arm and loft lengths for the truncated four feed arms with switch cones (T4FASC) configuration." EM Implosion Memo 40, Feb. 2010.

[7] Prashanth Kumar, Carl E. Baum, Serhat Altunc, Christos G. Christodoulou and Edl Schamiloglu, "Effect of the impedance of a bicone switch on the focal impulse amplitude and beam width." EM Implosion Memo 38, Feb. 2010.

Appendix-I

Normalized E_θ and E_ϕ electric field components for the T4FASC-CSS, T4FASC-CSS-SPVSHC and T4FASC-CSS-SPVCHC configurations.

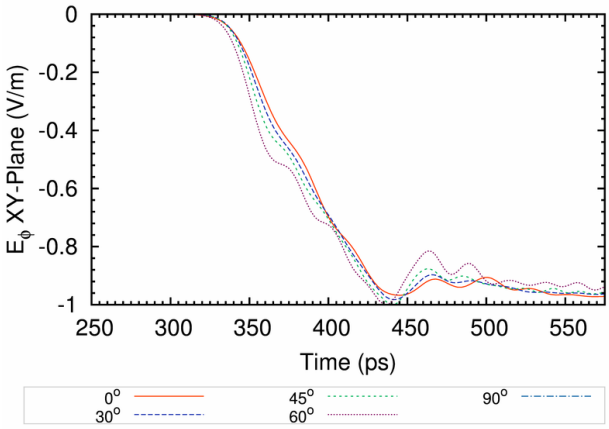

(a) Normalized E_ϕ in the $xy-$plane

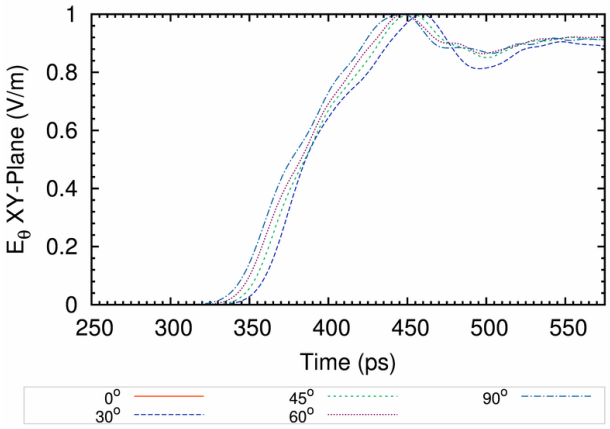

(b) Normalized E_θ in the $xy-$plane

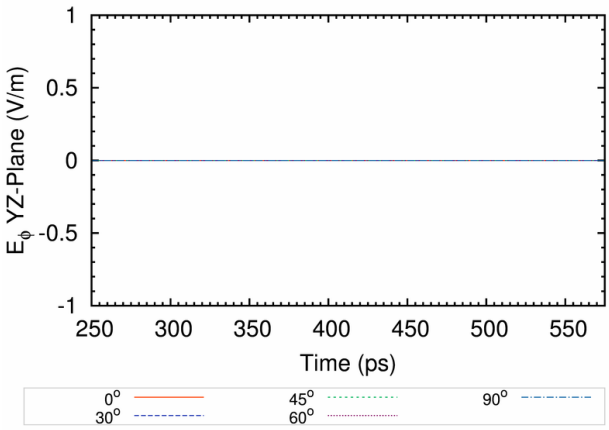

(c) Normalized E_ϕ in the -$yz-$plane

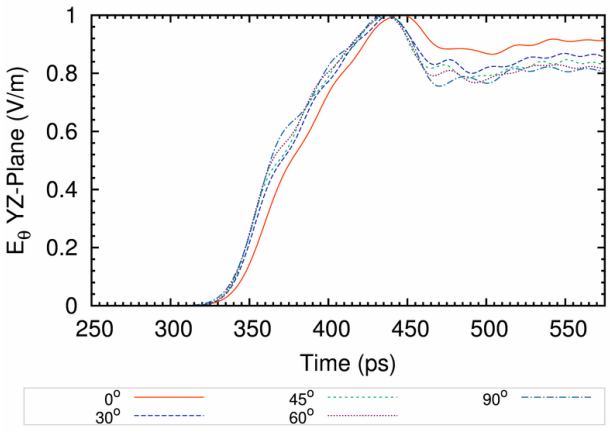

(d) Normalized E_θ in the -$yz-$plane

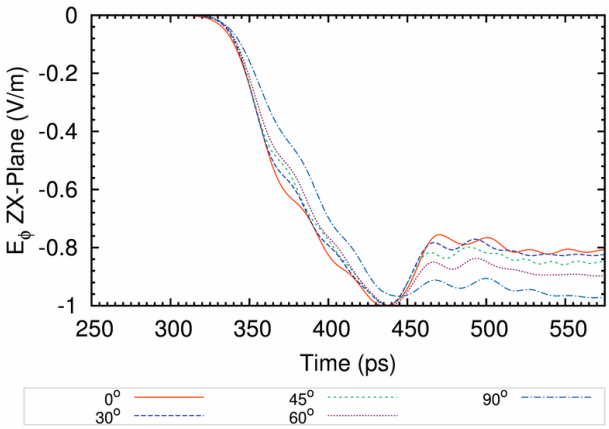

(e) Normalized E_ϕ in the -$zx-$plane

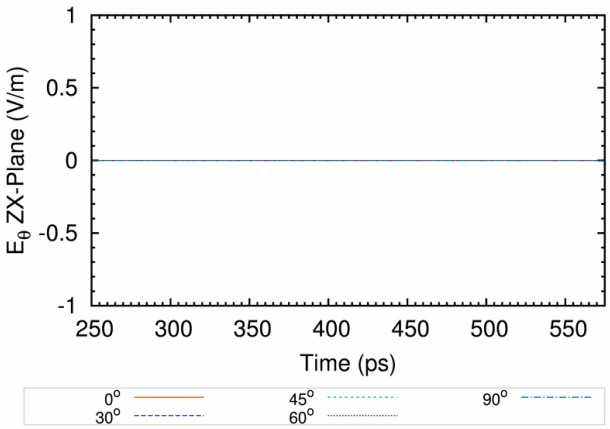

(f) Normalized E_θ in the -$zx-$plane

Figure 5.1: Normalized E_θ and E_ϕ components of the responses from the electric field probes on the $xy, -yz$ and $-zx$ planes for the T4FASC-CSS configuration.

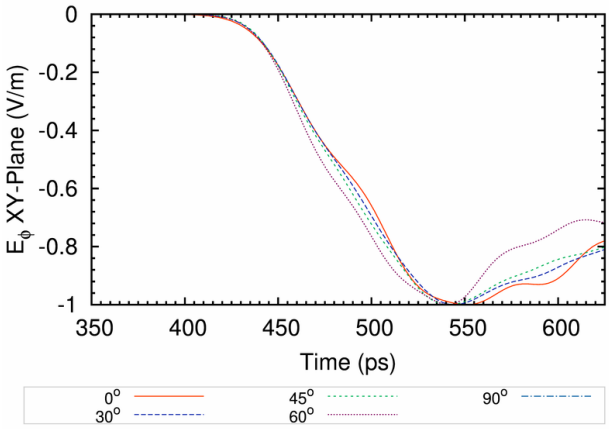

(a) Normalized E_ϕ in the $xy-$plane

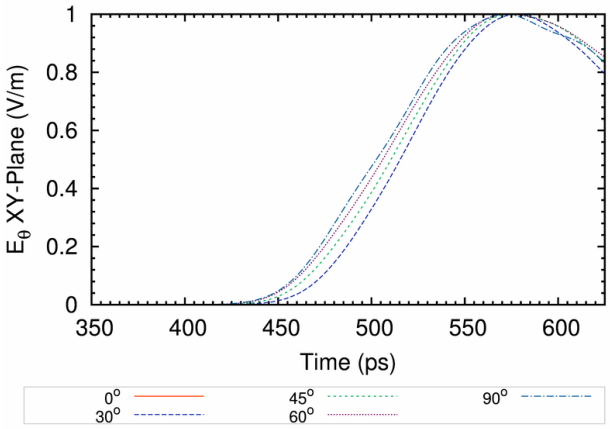

(b) Normalized E_θ in the $xy-$plane

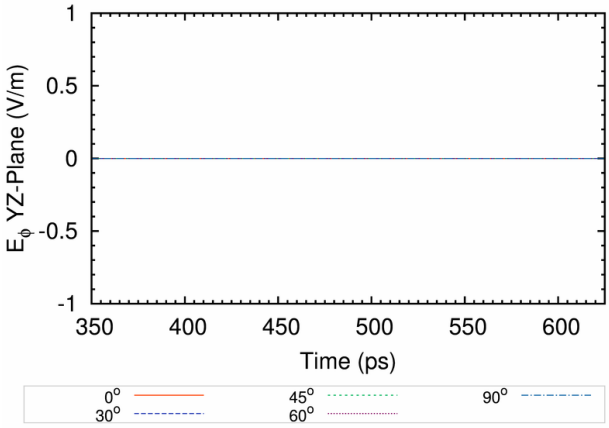

(c) Normalized E_ϕ in the -$yz-$plane

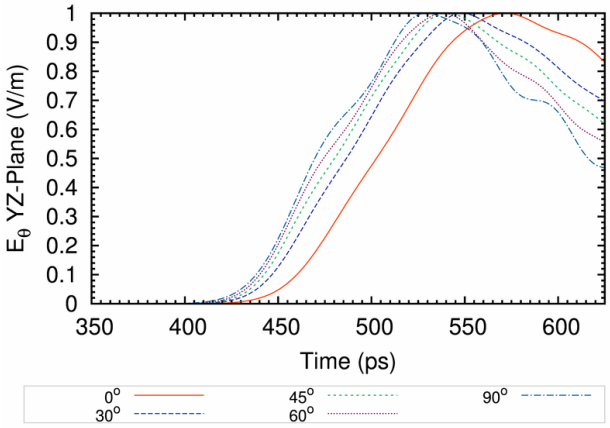

(d) Normalized E_θ in the -$yz-$plane

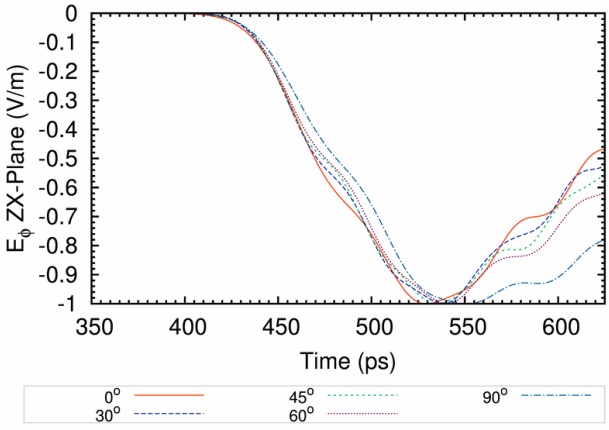

(e) Normalized E_ϕ in the -$zx-$plane

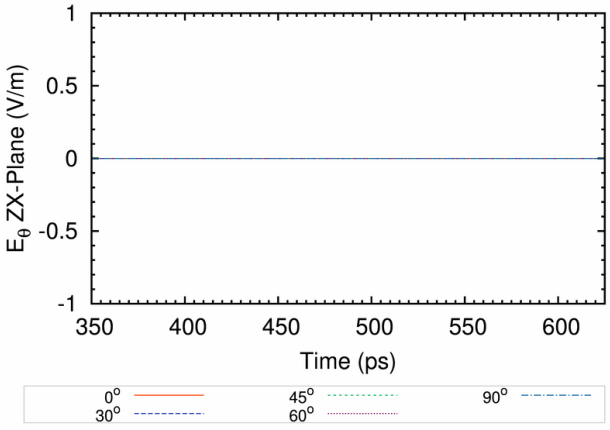

(f) Normalized E_θ in the -$zx-$plane

Figure 5.2: Normalized E_θ and E_ϕ components of the responses from the electric field probes on the $xy, -yz$ and $-zx$ planes for the T4FASC-CSS-SPVCHC configuration.

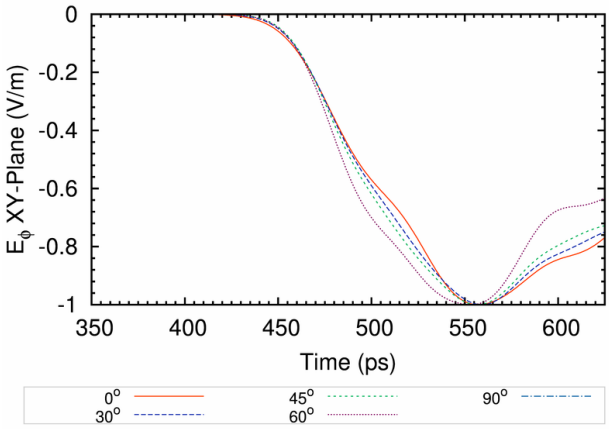

(a) Normalized E_ϕ in the $xy-$plane

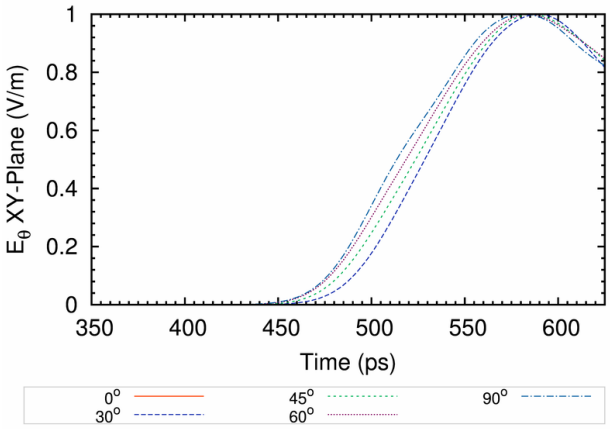

(b) Normalized E_θ in the $xy-$plane

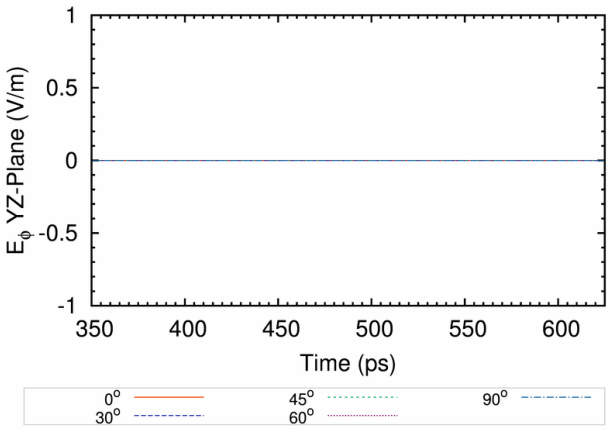

(c) Normalized E_ϕ in the -$yz-$plane

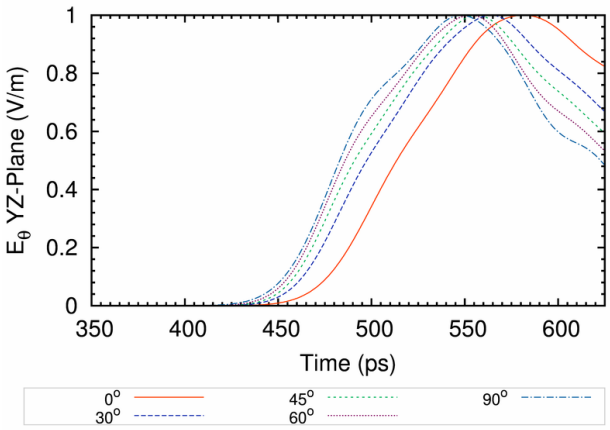

(d) Normalized E_θ in the -$yz-$plane

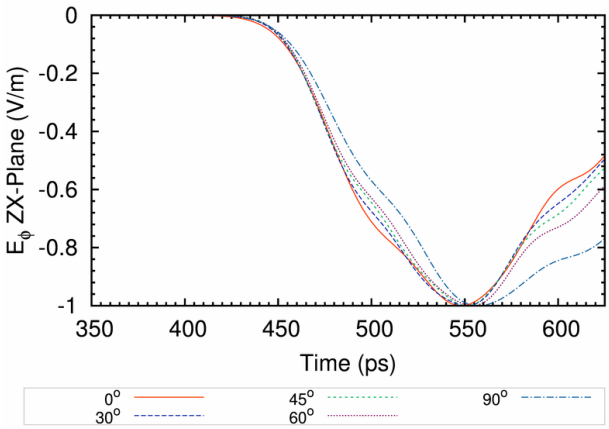

(e) Normalized E_ϕ in the -$zx-$plane

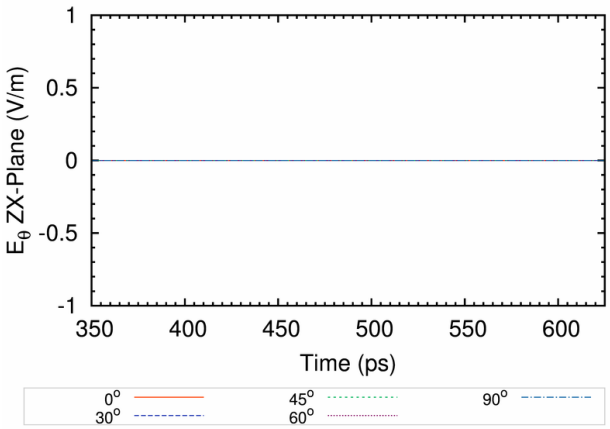

(f) Normalized E_θ in the -$zx-$plane

Figure 5.3: Normalized E_θ and E_ϕ components of the responses from the electric field probes on the $xy, -yz$ and $-zx$ planes for the T4FASC-CSS-SPVSHC configuration.

Appendix-II

Focal impulse waveforms and beam widths for the T4FASC-CSS, T4FASC-CSS-SPVSHC and T4FASC-CSS-SPVCHC configurations.

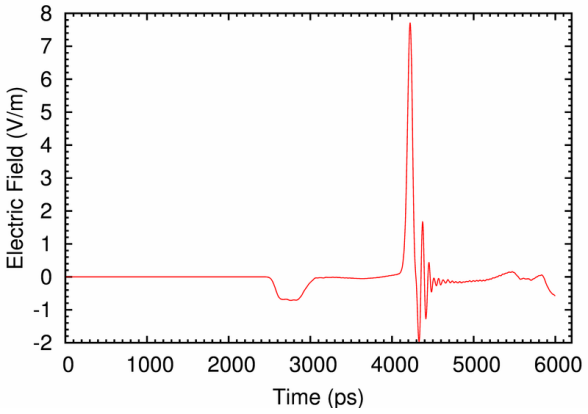

(a) T4FASC-CSS: Focal impulse waveform.

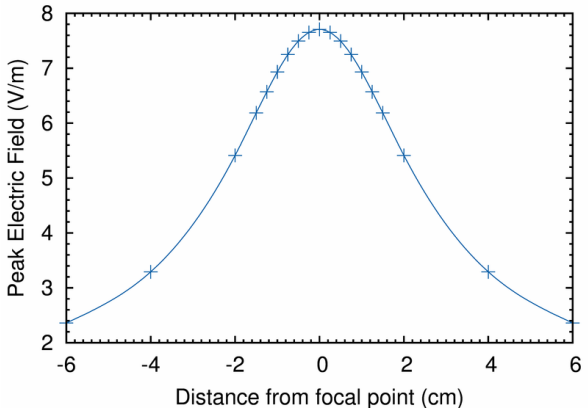

(b) T4FASC-CSS: Beam width.

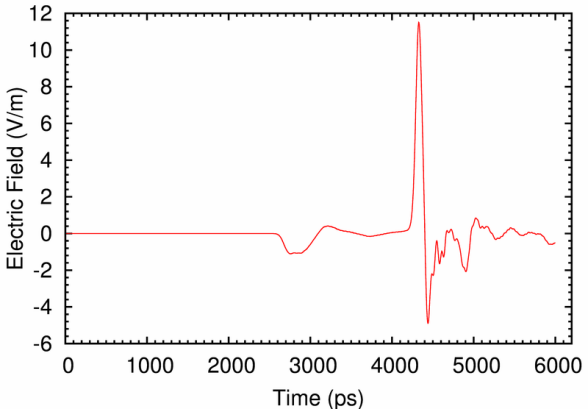

(c) T4FASC-CSS-SPVCHC: Focal impulse waveform.

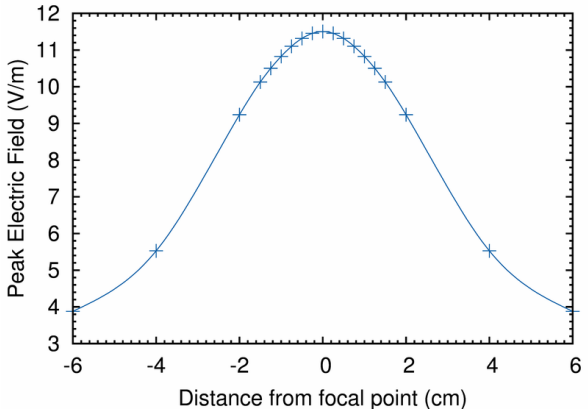

(d) T4FASC-CSS-SPVCHC: Beam width.

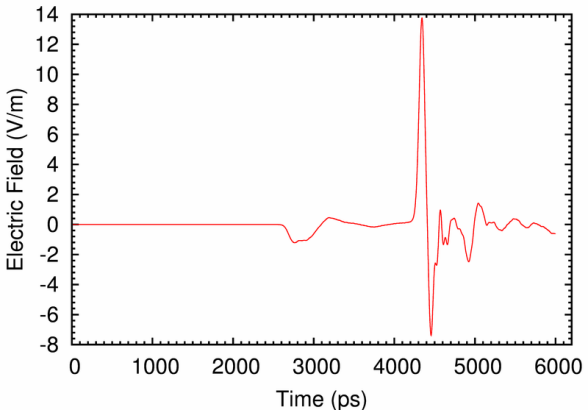

(e) T4FASC-CSS-SPVSHC: Focal impulse waveform.

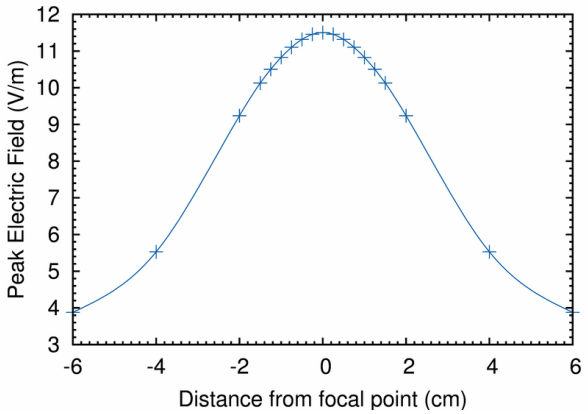

(f) T4FASC-CSS-SPVSHC: Beam width.

Figure 5.4: Electric field focal impulse waveforms and beam widths for the T4FASC-CSS, T4FASC-CSS-SPVCHC, and T4FASC-CSS-SPVSHC configurations .